

Review

A Review of Visible Light Responsive Photocatalysts for Arsenic Remediation in Water

Isabella Natali Sora ^{1,2,*} , Francesca Fontana ^{1,2} , Renato Pelosato ^{1,2}  and Benedetta Bertolotti ¹

¹ Department of Engineering and Applied Sciences, University of Bergamo, 24044 Dalmine, Italy; francesca.fontana@unibg.it (F.F.); renato.pelosato@unibg.it (R.P.); benedetta.bertolotti@unibg.it (B.B.)

² INSTM-Bergamo R.U., University of Bergamo, 24044 Dalmine, Italy

* Correspondence: isabella.natali-sora@unibg.it

Abstract: This review summarizes the progress over the last fifteen years in visible light reactive photocatalysts for environmental arsenic remediation. The design and performance of several materials including (1) doped and surface functionalized TiO₂, (2) binary composites combining TiO₂ with another semiconductor that absorbs visible light radiation or a metal (Pt), (3) ternary composites incorporating TiO₂, a conductive polymer that can retard electron-hole recombination and an excellent adsorbent material for the removal of As(V), (4) tungsten, zinc, and bismuth oxides, (5) g-C₃N₄ based catalysts, and (6) M@AgCl core-shell structures. These results show that long reaction time remains a major challenge in achieving high As(III) oxidation.

Keywords: arsenic; visible light photocatalysts; photocatalysis; photocatalytic wastewater treatment; advanced oxidation processes

1. Introduction

Arsenic is fairly abundant in Earth's crust, with a natural occurrence of 2–3 ppm on average, which makes it the 20th most abundant element in the crust. It exists in four main oxidation states, namely +V (arsenate), +III (arsenite), 0 (arsenic), and –III (arsine), of which the first two are the most abundant in the environment. In oxygenated water (such as surface waters) arsenic usually occurs in the form of As(V), whereas under reducing conditions, such as those often found in deep lake sediments or groundwater, the predominant form is As(III) [1]. Organoarsenic compounds, such as dimethylarsinic acid or monomethylarsonic acid [1], are also found in water.

Arsenic can diffuse in the environment from both natural and anthropogenic sources; the latter are derived from activities such as coal mining, smelting, fertilizers, and pesticides, and from the hide tanning, semiconductor, and aluminum industries [2]. However, arsenic contamination of drinking water is generally derived from geological sources. Bangladesh and India (West Bengal) are among the countries with the highest levels of contamination. Levels of arsenic above safe limits were also found locally in several countries in Europe, Australia, New Zealand, Brazil, and Canada [3].

Through prolonged exposure to arsenic-contaminated drinking water, the element accumulates in tissues. Signs of chronic arsenicism include dermal lesions, peripheral neuropathy, bladder, lung, and kidney cancers, urinary tract infections, peripheral vascular disorders, and skin cancer [2]. For acute toxicity, arsine is considered to be the most toxic form, followed by arsenites (As(III)), arsenates (As(V)), and organic arsenic compounds. The World Health Organization (WHO) estimated that about 180 million people in 50 countries have been exposed to toxic arsenic levels (at least 10 µg/L in drinking water). Consequently, the guideline value for the permissible limit for arsenic in drinking water according to WHO is 10 µg/L; however, every effort should be made to maintain levels as low as possible [4].



Citation: Natali Sora, I.; Fontana, F.; Pelosato, R.; Bertolotti, B. A Review of Visible Light Responsive Photocatalysts for Arsenic Remediation in Water. *Photochem* **2024**, *4*, 198–218. <https://doi.org/10.3390/photochem4020012>

Academic Editor: Ewa Kowalska

Received: 28 March 2024

Revised: 9 April 2024

Accepted: 10 April 2024

Published: 17 April 2024



Copyright: © 2024 by the authors. Licensee MDPI, Basel, Switzerland. This article is an open access article distributed under the terms and conditions of the Creative Commons Attribution (CC BY) license (<https://creativecommons.org/licenses/by/4.0/>).

For these reasons, abundant research has been devoted to the quest for remediation methods, especially for water treatment. It must be considered that none of the known technologies will work in every situation. The applicability of a given technology depends on the types and concentrations of the arsenic species, the pH of the medium, the presence of other dissolved species or organic contaminants, the volume of water to be treated, the cost, and the target value for concentration levels (namely, whether or not the obtained water must fit the requirements for drinking water).

Although the number of articles dealing with the application of photocatalysis to arsenic removal in water is relatively small, there are five recent reviews on the application of metal oxides for arsenic remediation in water under UV irradiation [1,5–8], none of which focused on visible light irradiation. One very recent review [9] deals with photocatalysis by both UV and visible light. Therefore, the present review emphasizes the visible-light-responsive performance of the semiconductor photocatalysts for arsenic remediation in water.

Methodologically, we decided to focus on photocatalytic methods of removal and to only take into consideration those papers meeting criteria that would ensure reproducibility of the results. We chose to take into consideration only those papers where all the following data are clearly stated: (i) As(III) or arsenic acid concentrations; (ii) catalyst concentration (where applicable); (iii) required time; (iv) characteristics of the light source; and (v) percentage of removed pollutant.

2. Conventional Remediation Techniques

In many cases, arsenic levels in groundwater are much higher than the allowed limit of 10 µg/L; therefore, a variety of methods are used for decontamination. Mostly, they can be grouped into the categories of adsorption and ion exchange, coagulation–precipitation processes, membrane processes, and bioremediation.

As the various forms of arsenic undergo acid–base equilibria, pH is of paramount importance in determining whether arsenic will be present in neutral or ionic form [1,10], as shown in Figure 1.

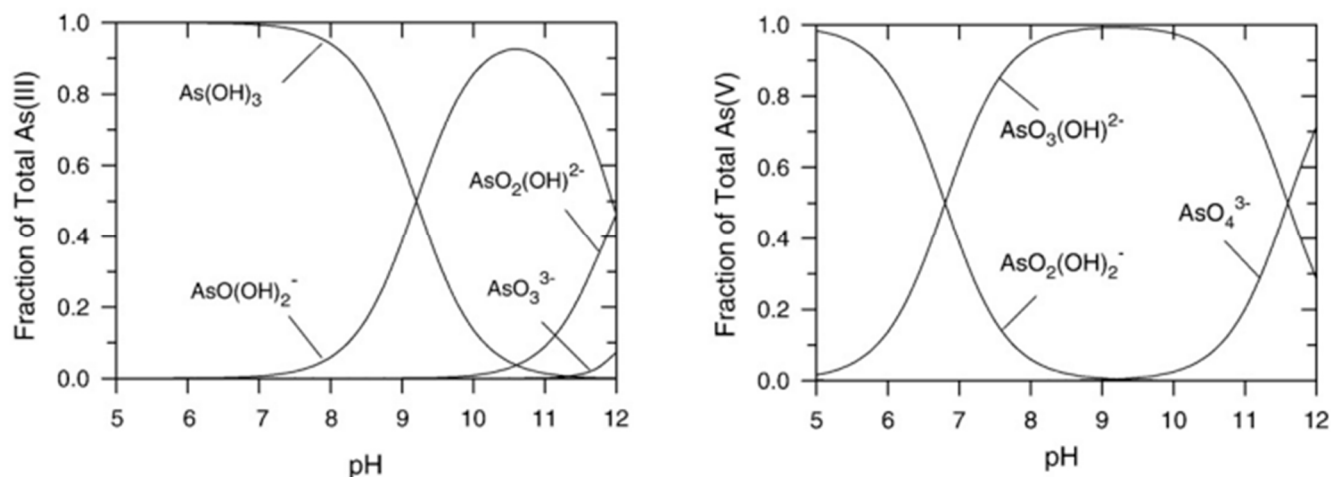


Figure 1. Arsenic speciation in water as a function of pH: As(III) (left) and As(V) inorganic species (right). Reprinted with permission from Ref. [1]. Copyright 1999, Elsevier.

When the problem to be addressed is the treatment of drinking water, pH must be close to neutrality, at which value As(III) is mainly in a neutral form, while As(V) is in anionic form. In general, as arsenite is electrically neutral at a pH of 9.2, most current arsenic remediation methods for drinking water, which exploit the presence of surface charge, typically perform better in removing the less toxic As(V); therefore, peroxidation usually has to be applied for arsenite removal [11].

2.1. Oxidation

Oxidation is a preliminary technique used to convert As(III) to As(V); the latter must then be removed from water using a physical technique. The preferred oxidizing techniques include the use of chemicals, electrochemistry, and photochemistry.

Chemical oxidants include different species, such as ozone, chlorine, and KMnO_4 , which can rapidly and completely oxidize As(III) at concentrations of $50 \mu\text{g/L}$ or higher. However, in some cases, pH must be kept above 7.5, and other contaminants, such as sulfides, may interfere, slowing the process. Other oxidants, such as oxygen, air, chloramine (NH_2Cl), chlorine dioxide, hydrogen peroxide, and ferrate, generally require longer contact times and fail to achieve complete oxidation of As(III) [12,13]. Hypochlorite may also be used, but complete oxidation requires a concentration of $500 \mu\text{g/L}$ [12,14]. If the oxidizing species is a solid, it also acts as an adsorbent for the resulting As(V) [13,15,16]. The oxidation of As(III) with H_2O_2 and Fe(II) is important in natural and technical systems at pH values up to 8, below which As(III) is not oxidized at appreciable rates by H_2O_2 alone [17].

One effective solution was to pump oxygenated water into the aquifer prior to arsenic removal to reduce As concentrations to $<10 \mu\text{g/L}$ [18].

As(III) oxidation can also be achieved by biological methods by exploiting bacteria or algae [19].

Electrochemistry is a viable system for the anodic oxidation of arsenite without the use of noxious chemicals [20]. Oxidation may be direct, where the As(III) species are directly adsorbed on the electrode surface and oxidized, or indirect if the process involves the electrochemical generation of an oxidizing species, such as O_2 [21]. A huge amount of research is presently devoted to the quest for an efficient electrode material [15,22]. Electrochemical methods seem promising owing to low energy consumption and good As removal, even down to $<1 \mu\text{g/L}$, although their efficacy in groundwater is lower than in synthetic water in several instances [20].

Photochemical oxidation of As(III) can be achieved when light-absorbing substances such as H_2O_2 , Fe(III) complex, $\text{NO}_3^-/\text{NO}_2^-$, and I^- , produce transient high-energy species under UV radiation [11]. Photocatalytic oxidation has often been used [23], in many cases by TiO_2 -based photocatalysts; however, owing to its wide bandgap, TiO_2 is only activated by UV light, thus allowing the exploitation of only a small fraction of solar light or requiring the use of UV lamps. Photocatalysis by visible light is detailed below.

Table 1 sums up the main oxidation methods used for As(III), with their main advantages and drawbacks.

Table 1. Main oxidation methods to convert As(III) into As(V).

| Oxidation Method | Advantages | Disadvantages | Ref. |
|-----------------------|---|--|------------|
| chemical oxidation | suitable for high [As(III)], fast and complete for some oxidants, some oxidants may act as adsorbents | need for stoichiometric chemicals, potentially toxic residues, efficiency may be strongly pH dependent, possible interference by other substances present in groundwater | [12,13,18] |
| in situ oxidation | simple, cheap, effective ($<10 \mu\text{g/mL}$), no sludge | very few reported examples | [18] |
| electrochemistry | no chemicals required, high pH groundwater is reduced to $\approx\text{pH } 7$, viable cost | need for electrochemical apparatus, possibility of formation of noxious by-products, lower efficacy in groundwater than in synthetic water | [15,20] |
| biochemical oxidation | biocompatible, algae may act as adsorbents | need for selected strains of bacteria or algae and controlled temperature, proved effective only in laboratory conditions | [19] |
| photocatalysis (UV) | efficient, no chemicals required | need for UV radiation, possible interference from other ions present in groundwater | [13,23] |

In the following paragraphs, the main conventional techniques that can be applied after oxidation for the removal of arsenic from water are described.

2.2. Adsorption

The most widely used system for arsenic removal from groundwater is adsorption, due to its simple operation, potential for regeneration, and minimal toxic sludge generation. Processes based on the use of natural, locally available adsorbents are considered to be more accessible for low-income countries, as they have a smaller investment cost and a lower environmental impact (CO₂ emission) [24]. Adsorption of As is highly dependent on several parameters, including pH, the presence of other cations, particle size, surface porosity, the oxidative state of As(III or V), contact time, and adsorbent dosage.

The optimal conditions are determined by the types of surface functional groups and surface charges present on the adsorbent being used. A wide variety of materials has been used for arsenic adsorption. Among them, rocks, minerals, and other materials containing iron oxides or hydroxides [25] and/or alumina, such as red mud from the treatment of bauxite, carbon-based materials such as activated carbon [26], which is frequently obtained during combustion of a wide variety of locally available agricultural wastes, biochar [27–29] graphene [30], and a huge variety of polymer-based materials and composites [31]. Frequently, these materials are manufactured in the form of nanoparticles, which have large surface areas, highly porous surfaces, and large numbers of active sites [8]. Other low-cost materials for arsenic adsorption are those classified as biosorbents, among which are biopolymers such as chitosane, alginate, or cellulose, raw waste material from agricultural activities such as rice husks, biomass from wood processing [32], and microalgae and fungal biomass [24]. All these materials have the advantage of being locally available and easily manageable, even in low-income countries.

An intrinsic problem of this remediation approach is the need for subsequent disposal of the contaminated sorbent. In principle, two approaches are possible: (a) desorption of arsenic from the adsorbent medium, to recover and reuse the latter and/or to obtain and utilize the arsenic itself; and (b) dumping of the contaminated adsorption material. As arsenic does not have many industrial applications, its recovery is usually not economical, so most of the time it is disposed of. However, it cannot be destroyed, and incineration of the sorbent is not viable due to the high volatility of arsenic compounds. Therefore, safe management of the spent sorbent medium requires prior application of stabilization/solidification techniques to avoid leaching of toxic compounds from landfills. For instance, it can be incorporated into building materials or in a cementitious binder [33]. Iron hydroxides can be thermally treated in order to promote arsenic fixation and, therefore, safer disposal of the solid residue [34]. Some instances instead use the recovery approach: about 85% of As adsorbed on δ -FeOOH nanoparticles was recovered by treatment with NaOH solution, to be used as a precursor for the synthesis of Ag₃AsO₄, which is a material with outstanding photocatalytic activity [35]. Desorption methods were also developed for the reuse of the sorbent material [36]. A recent review [2] dealt with the disposal of sorbents, whereas another [37] investigated plants performing arsenic adsorption from water in continuous mode and the latest progress in the regeneration and recovery of arsenic. The disposal of the exhausted bed was also discussed.

2.3. Precipitation

The precipitation methods are mainly used for the remediation of heavily arsenic-loaded wastewater, such as those derived from mining and related activities. In industrial wastewater, precipitation of As(III) in the form of sulfide As₂S₃ is almost complete at pH 2 [38]. Coagulation/flocculation is usually obtained by iron or aluminum salts used as flocculants. The technology of coagulation–flocculation is simple, only common chemicals are used, installation costs are low, and it can be easily applied to large volumes of water. During this process, As(V) is removed more effectively than As(III); however, As removal is hindered by the presence of sulfates, silicates, and phosphates, and simple setting of the

solution is not sufficient for effective decontamination, and filtration is a necessary step [39]. During the precipitation processes, often owing to low selectivity, a large amount of sludge is produced [40], which is usually disposed of in landfills. Precipitation is sometimes proposed as a method for the treatment of wastewater produced by the management of arsenic-laden waste created during the regeneration of exhausted adsorbents [41].

As in the case of adsorption, the production of solid waste with high arsenic content during precipitation poses leaching problems [42]; however, as the amount of arsenic in this type of waste is important, remediation techniques are also frequently directed to the recovery of arsenic for reuse [43,44].

2.4. Membrane Technologies

Membrane technology is a promising area for arsenic removal from water. The most commonly developed membrane separation processes are reverse osmosis (RO), electrodialysis (ED), microfiltration (MF), ultrafiltration (UF), and nanofiltration (NF). Microfiltration, ultrafiltration, nanofiltration, and reverse osmosis are pressure-driven processes, whereas electrodialysis is an electro-driven process. For arsenic remediation, the most appropriate technique is nanofiltration due to its ability to eliminate multivalent ions in water [45]. A recent review [46] compared the various membrane techniques and discussed the research trends, indicating advantages and drawbacks, the latter of which were typically the issues of low durability [47] and fouling. Fouling is the deposition of solutes on the membrane surface and within pores, and it causes mass transfer resistance, low water flux, and low selectivity [45]. In another review [39], emergent membrane-based technologies such as forward osmosis, membrane distillation, and electrodialysis were discussed.

2.5. Other Techniques

Ion exchange was realized using a vast number of materials, such as metal–organic frameworks [48] or polymeric ion exchange resins containing dispersed metal oxide nanoparticles [49]. Resins require periodic regeneration via treatment with solutions of appropriate counterions and must eventually be disposed of in landfills, where they should not give rise to leachate.

Bioremediation using the biomass of bacteria, algae, fungi, and yeast has gained much attention from researchers in the last few decades as an environmentally friendly and cost-effective approach [50]. Arsenic-resistant bacterial strains can be genetically engineered for better performance. Microbial consortia, namely organized collectives of microorganisms, either natural or engineered, can work synergistically [51].

Although arsenic bioremediation using bacteria can be very effective within laboratory conditions, bacterial ecology in the environment may present important differences with respect to their behavior under controlled parameters. Hence, it is essential to develop bioremediation systems in field applications to enhance their commercial viability.

Electrochemical methods are interesting because of their flexibility, environmental compatibility, low cost, and high efficiency. They can be distinguished using separation and oxidation methods [21]. Separation methods include electrocoagulation, electrodialysis, and electrosorption.

Directional solvent extraction with decanoic acid was applied at low temperature to achieve purification from arsenic to meet drinking water standards [52].

Generally speaking, evaluation of the viability of a given decontamination technique depends on a vast number of factors, including economic issues, acceptability by the users, management of the resulting waste, ease of maintenance of the plant, and so on, and considerations may vary greatly based on the location of the plant and the characteristics of the contaminated water [53]. Particularly in low-income countries, even where decontamination plants have been built, their long-term efficiency is often not guaranteed [54], and residents often discontinue their use of water treatment plant for various reasons [55].

3. Heterogeneous Photocatalysis for the Removal of Arsenic in Water

Heterogeneous photocatalysis, which mainly refers to semiconductor photocatalysis or semiconductor-sensitized photoreactions, is considered a promising alternative to conventional processes used for the removal of toxic As(III) from water. The process mainly oxidizes As(III) into As(V), which may be then removed from the solution either by precipitation or by the addition of a suitable adsorbent, typically iron oxides such as Fe₂O₃ and Fe₃O₄.

In the photocatalytic process, a chemical reaction is activated or its rate is increased when a semiconducting photocatalyst is irradiated using photons with energy that matches the band gap energy of the semiconductor, resulting in the formation of excited electron-hole ($e^- - h^+$) pairs. The excited electrons are promoted from the valence band (VB) to the conduction band (CB), thereby generating holes in the VB (Figure 2) [56]. Owing to the band bending, electrons and holes move to the surface of the semiconductor, where, in the absence of electron and hole scavengers, their recombination occurs in few nanoseconds. Recombination is avoided if a proper scavenger or surface defect state is available to trap the electron-hole pairs, and in this case, the electron and hole can be involved in thermodynamically facilitated electron transfer reactions with the solvent or other species. Adsorbed water or hydroxyl groups present on the semiconductor surface can be oxidized by h^+ , generating HO^\bullet (Equation (1)), while adsorbed $O_{2\ ads}$ can be reduced by e^- , generating superoxide radicals, $O_2^{\bullet-}$ (Equation (2)):

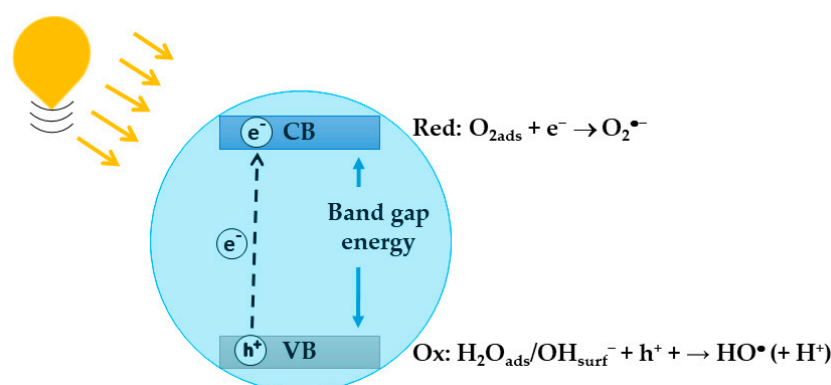
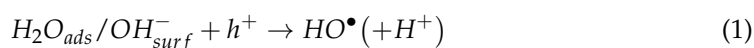
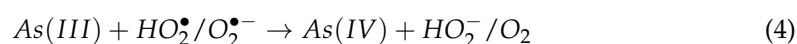


Figure 2. Schematic representation of the formation of excited electron-hole pair.

The mechanism of photocatalytic oxidation of As(III) has been studied for many years, and research has focused on determining the major oxidant in the system, either $O_2^{\bullet-}$, HO^\bullet , or h^+ [57,58]. The oxidation of As(III) to As(V) proceeds through mono-electronic steps with the formation of As(IV), as described by the following equations:



Subsequently, As(IV) is readily oxidized to As(V) by $O_2^{\bullet-}$, HO^\bullet , or molecular O_2 [59]. With all these oxidants, the heterogeneous photocatalytic process is highly efficient at transforming As(III) into As(V) [60,61].

The most studied material for the photocatalytic oxidation of As(III) in water under UV light is TiO₂ coupled with an iron oxide, such as α -Fe₂O₃, which acts as an adsorbent of As(V), improving the total arsenic removal. Although the band-gap energy of α -Fe₂O₃ is about 2.0 eV, TiO₂/Fe₂O₃ is not efficient in the As(III) oxidation reaction under visible-light irradiation, because Fe₂O₃ is a rather poor photocatalyst due to rapid electron–hole recombination [62].

A good photocatalytic material must show chemical stability under a wide variety of environments. Metal oxide semiconductors with a band gap in the range of 2–4 eV generally possess this important property. In addition to being chemically robust, a good photocatalyst should exhibit other important properties such as (i) a high surface-to-mass ratio, (ii) efficient absorption of light in a useful range of frequencies, and (iii) efficient separation and transportation of photogenerated charge carriers. To achieve the first feature, the surface-area effects of metal oxides are tailored by preparing nanoparticles using suitable synthetic methods (such as hydrothermal/solvothermal and sol–gel syntheses) or, alternatively, as a result of deposition onto a nanostructured film. The importance of the second property is related to the fact that exploiting a light source in the visible region of the electromagnetic spectrum would make the management of wastewater treatment plants simpler and more economical. Several strategies are adopted to extend the optical response of photocatalytic materials to the visible region: among others, doping with metal and/or non-metal elements, surface functionalization, composites, and junction coupling [63,64]. In particular, nano-heterojunctions could enhance visible light absorption and induce band bending and the formation of an internal electric field [65]. Consequently, owing to specific band alignment and spatial charge separation, the photoactivity is improved.

3.1. Photocatalytic Oxidation of As(III) Using Modified TiO₂

Titanium dioxide (TiO₂) is an *n*-type semiconductor. It has been widely studied as a photocatalyst in the oxidative degradation of organic and inorganic water pollutants [66,67]. The interaction of TiO₂ with UV radiation generates electron–hole pairs, which activate surface reactive processes [59,61]. Among the three common crystalline polymorphs of TiO₂ (rutile, anatase, and brookite) the anatase phase exhibits higher photocatalytic behavior for oxidation processes. The relatively wide bandgap of TiO₂ anatase, $E_g = 3.2$ eV corresponding to a threshold of 390 nm, hinders the exploitation of solar light in photocatalytic reactions. Moreover, the high recombination probability of the photogenerated electron–hole pairs results in low quantum efficiency of photocatalyzed reactions, which is a feature present in all semiconductor photocatalysts. Different approaches have been developed to modify the process involving light harvesting and excitation to increase visible light absorption of TiO₂ and to maximize electron–hole separation. A widespread strategy consists of doping TiO₂ with metal and/or non-metal elements; this is achieved through the incorporation of different elements into the TiO₂ crystalline lattice, resulting in modified electronic properties. No previous literature discussing the photocatalytic oxidation of As(III) using TiO₂ modified by a physical method (such as ion implantation) was found. Table 2 lists the examples of visible-light-activated chemically modified TiO₂ covered in this review. A brief description of their performance for As(III) oxidation is also provided. Fe-doped TiO₂ [68] outperformed other types of doped TiO₂ such as N-doped TiO₂ fiber [69], N–S co-doped TiO₂ [70], and Er-doped TiO₂ [71]. It is worth noting that in ref. [68], a very high (3 g/L) concentration of Fe-doped TiO₂ was used to remove 100% of As(III) in 30 min. TiO₂ doped with Er³⁺ 2.0 mol% and reduced graphene oxide (rGO) 10.0 mol% degrades 100% of arsenic acid (*p*-ASA) in 50 min under visible light, and the resulting arsenic (mainly As(V)) is rapidly removed from the solution owing to the strong adsorption of rGO to inorganic arsenic [71].

Some studies that were carried out with the aim of investigating the mechanism of photocatalytic oxidation of As(III) in the presence of TiO₂ were performed under visible-light irradiation and pH = 3 [72,73]. The visible-light-induced oxidation on dye-sensitized Pt-TiO₂ (~80% in 60 min) [73] is as fast as the UV photooxidation on Pt-loaded TiO₂.

Nanostructured TiO₂ nanotubes prepared by potentiostatic anodization of a titanium foil, combined with Pt-loading, are capable of harvesting visible light because of localized surface plasmon resonance (SPR) of Pt nanoparticles. Qin et al. reported that Pt nanoparticles on TiO₂ nanotubes induce the oxidation of 83% of As(III) in 280 min [74].

Table 2. As(III) oxidation to As(V) over modified TiO₂ photocatalysts under visible light.

| Photocatalyst | pH | Light Source | As(III) (μM) | Catalyst (g/L) | As(III) Oxidized (%) | Time (min) | Ref. |
|--|------|--|---------------------|----------------|----------------------|------------|------|
| (Ru ^{II} /L3) dye-sensitized Pt-loaded TiO ₂ | 3 | Xe 300 W λ > 420 nm | 500 | 0.5 | ~80 | 60 | [73] |
| 4-chlorophenol/TiO ₂ system | 3 | Xe 300 W λ > 420 nm | 200 | 0.5 | ~90 | 300 | [72] |
| Pt-loaded TiO ₂ nanotube | 7 | 300 W halogen λ > 420 nm | 45.4 | foil | 83 | 280 | [74] |
| N-doped TiO ₂ fiber | 7 | Xe 300 W λ > 420 nm | 133 | 0.5 | 100 | 90 | [69] |
| Fe-doped TiO ₂ | n.a. | LED 400–600 nm | 80 | 3 | 100 | 30 | [68] |
| N–S co-doped TiO ₂ | 9 | LED 650 W/m ² 430–650 nm | 46 (<i>p</i> -ASA) | 1 | 98 | 300 | [70] |
| 2 mol% Er-doped TiO ₂ | n.a. | Xe 500 W λ > 400 nm | 23 (<i>p</i> -ASA) | 0.1 | ~70 | 90 | [71] |
| Er ³⁺ -rGO co-doped TiO ₂ | n.a. | Xe 500 W λ > 400 nm | 23 (<i>p</i> -ASA) | 0.1 | 100 | 50 | [71] |

As mentioned above, an adsorption step takes place before the reaction step. There is an attractive interaction between particles with opposite electric charges. The solution pH significantly affects the charge of the surface particles. The pH of zero-point charge (zpc) is the value at which the material surface is neutral (uncharged). Below this value, the photocatalyst is positively charged and attracts negative species. At pH values above the zpc, the photocatalyst surface is negatively charged and attracts positive species. Although the large band gap of TiO₂ limits the utilization in visible light, many studies examined the arsenic adsorption performance of Degussa P25 TiO₂. The results showed that at pH 4, adsorption for As(V) is much higher than for As(III) because of the negative and neutral speciation of As(V) and As(III) (see Figure 1), respectively. As(V) desorbs more effectively as pH increases, and at pH 9, the adsorption of As(III) is higher than As(V) [75]. The maximum adsorption capacity for As(III) (89 μM) is 2.4 mg/gTiO₂, and that for As(V) is 9.7 mg/gTiO₂ at pH 6.3 [76].

Colored TiO_{2-x} shows photoactivity under visible light. As shown in Figure 3, As(III) adsorption diminished above zpc (at pH 6.3) under visible light owing to the conversion of As(III) to As(V) by photocatalytic oxidation (a conversion rate of about 2.85 mgAs/g h) [77].

3.2. Photocatalytic Oxidation of As(III) Using TiO₂-Based Nanocomposites

The design of TiO₂-based nanocomposites is the most frequently used strategy to increase the efficiency of photocatalytic reaction under visible-light irradiation and, at the same time, to enhance the pollutant removal capacity. Interfacial interactions between the phases forming a nanocomposite make the physical properties different from those of its individual components. WO₃ absorbs solar radiation better than TiO₂ owing to its smaller band-gap energy of about 2.6 eV [78]. When TiO₂ is coupled with WO₃ (TiO₂/WO₃ nanocomposite), the photo-generated electrons of WO₃ are transferred to the TiO₂ conduction band, thus generating holes in the WO₃ valence band [79]. TiO₂/WO₃ composite oxidizes about 75% of As(III) in 60 min, while V₂O₅@TiO₂ composite with a core-shell

sphere microstructure oxidizes 92% of As(III) in 80 min [80]. Hydrogenated black TiO₂ (HBTiO₂, anatase) and rutile-based inorganic hollow microspheres (RBIHM) oxidize 70.3% of arsenite in 30 min [81]. Coupling HBTiO₂/RBIHM with MoS₂ results in superior As(III) photooxidation of 96.6% in 30 min under visible light [81]. Repeated experiments of HBTiO₂/RBIHM-MoS₂ maintain 91.4% of As(III) photooxidation after 5 cycles.

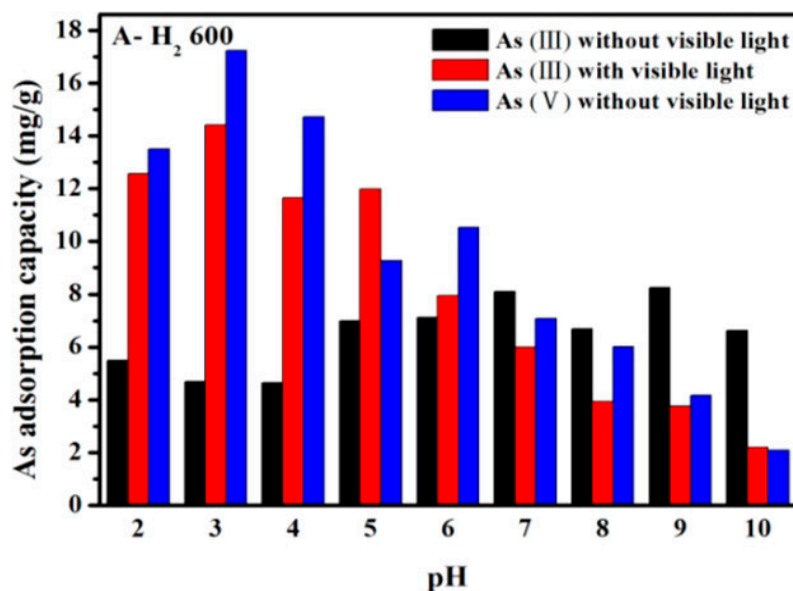


Figure 3. Effect of pH on arsenic adsorption on TiO_{2-x} with and without visible light. Reprinted with permission from ref. [77]). Copyright American Chemical Society 2020.

Ternary composites incorporating (i) TiO₂, (ii) a conductive polymer to retard electron-hole recombination, and (iii) an excellent adsorbent material for the removal of As(V) were investigated. Examples include γ -Fe₂O₃/polyaniline/TiO₂ [82], MWCNT/polyaniline/TiO₂ [83], Fe₃O₄/polyparaphenylene diamine/TiO₂ [84], and γ -Fe₂O₃/polythiophene/TiO₂ [85]. As shown in Table 3, the best results were obtained by γ -Fe₂O₃/polythiophene/TiO₂, which oxidizes 99% of As(III) in 300 min and simultaneously adsorbs 90% of As(V) [85]. Recently, graphitic carbon nitride (g-C₃N₄), which absorbs visible light (band-gap energy of 2.7 eV), but is a poor arsenic sorbent, was coupled with B-doped TiO₂, showing a removal efficiency of 92% of As(III) in 300 min [86]. The literature reports the effect of oxyanions that are frequently present in water on photocatalysis reaction rates through competitive adsorption and surface-site blocking [87,88]. In particular, NO₃²⁻ and CO₃²⁻ have a weak inhibitory effect on the adsorption ability of γ -Fe₂O₃@polyaniline@TiO₂, while the removal capacity of As decreased by 17% in the presence of SO₄²⁻ and by 45% in the presence of PO₄³⁻ [82].

3.3. Photocatalytic Oxidation of As(III) Using WO₃, ZnO, and Bismuth Oxides

Although the semiconductor oxide most widely used as photocatalyst is TiO₂ because of its low cost, stability, and reactivity, it is effective only under UV-light irradiation, which limits its utilization with solar light and increases costs and management problems. In addition to studying many types of modifications to widen the absorption range of TiO₂, other semiconductor oxides that can absorb light in the visible range were studied.

Tungsten (VI) trioxide was studied as a photocatalyst because of its effective oxidation capacity of valence band (VB) holes, strong absorption of solar radiation, small band gap (2.4–2.8 eV), high oxidation power of valence band (VB) holes (+3.1–3.2 V_{NHE}), and nontoxicity [89].

Table 3. As(III) oxidation to As(V) over TiO₂-based nanocomposite photocatalysts under visible light. @ indicates core–shell structure.

| Photocatalyst | pH | Light Source | As(III) (μM) | Catalyst (g/L) | As(III) Oxidized (%) | Time (min) | Ref. |
|---|--------|--|--------------|----------------|----------------------|------------|------|
| TiO ₂ /WO ₃ | 3 | 230 W EB-1750 Epson | 200 | 0.4 | ~75 | 60 | [79] |
| V ₂ O ₅ @TiO ₂ | 4 | Xe 300 W λ > 420 nm | 26.7 | 0.8 | 92 | 80 | [80] |
| HBTiO ₂ /RBIHM * | 10 | DH-2000 deuterium tungsten halogen 1060 W/m ² λ > 420 nm | 0.76 | 0.5 | 70.3 | 30 | [81] |
| HBTiO ₂ /RBIHM-MoS ₂ * | 10 | DH-2000 deuterium tungsten halogen 1060 W/m ² λ > 420 nm | 0.76 | 0.5 | 96.6 | 30 | [81] |
| γ-Fe ₂ O ₃ @PANI@TiO ₂ | 8.5–10 | n.a. | 67 | 1.0 | ~89 | 300 | [82] |
| MWCNT/PANI/TiO ₂ | 5 | Xe 500 W λ > 380 nm | 267 | 0.5 | ~52 | 300 | [83] |
| Fe ₃ O ₄ @PpPDA@TiO ₂ ‡ | 6 | Xe 500 W λ > 380 nm | 267 | 0.5 | ~78 | 300 | [84] |
| γ-Fe ₂ O ₃ /PTh/TiO ₂ # | 6 | Xe 500 W Visible light | 26.7 | 0.5 | 99 | 300 | [85] |
| B-doped TiO ₂ /g-C ₃ N ₄ | 5 | Xe 500 W Visible light | 26.7 | 0.5 | 92 | 300 | [86] |

* HBTiO₂ = hydrogenated black TiO₂. RBIHM = rutile-based inorganic hollow microspheres. ‡ PpPDA = poly-paraphenylene diamine. # PTh = polythiophene. n.a. = not available.

The photocatalytic oxidation of As(III) to As(V) on WO₃ primarily proceeds through two-hole transfer, while hydroxyl radical (HO•) and hydrogen peroxide (H₂O₂) are only marginally involved in the oxidation of As(III) to As(V) [90]. However, the rapid recombination of photo-generated electron–hole pairs reduces the catalytic activity and calls for modifications aimed at increasing the efficiency of the electron–hole separation. As shown in Table 4, platinization is one such modification [89], the purpose of which is to enable O₂ to serve as an electron acceptor despite the insufficient reduction potential of the conduction band electrons in WO₃. The catalytic system was tested on several types of substrate; As(III) was in all cases successfully converted to As(V), but the oxidation is much faster with the platinized catalyst. Another way to increase the efficiency of WO₃ is to add Cu²⁺ ions or CuO as a co-catalyst [91]. It was established that the presence of Cu²⁺ increases the arseniate oxidation rate by 3.6 times, while the rate for CuO increases by 2.3 times compared with pure WO₃. In addition, pH plays an important role in increasing the oxidation rate of As(III): in the case of Cu²⁺–WO₃, oxidation takes place at an acidic pH and is much faster than with CuO–WO₃ at basic pH [91].

Zinc (II) oxide is another oxide that has attracted the attention of researchers who are studying new, economically competitive methods for the oxidation of arsenic (III). This compound shows peculiar characteristics, such as a direct and wide band gap in the near-UV spectral region, strong oxidation ability, good photocatalytic properties, and a high free-exciton binding energy [92]. ZnO is also more affordable than TiO₂. To make it active even under visible-light irradiation and to improve its photocatalytic performance, the literature suggests different solutions, including the introduction of different types of metal dopants into ZnO (Table 5). Cu is a cationic dopant that leads to a lower band gap energy value compared with undoped ZnO. The tests showed the complete conversion of As(III) to As(V) in the presence of Cu-doped ZnO under visible light [93], which did not happen in the presence of pure ZnO under the same conditions. The same result was also obtained using solar-simulated radiation. In 2021, to develop a catalyst that was

simple to remove, Cu-doped ZnO was supported on polystyrene pellets [93]. The excellent performance of the photocatalyst, as proved in a previous paper [93], was also provided in this case. It was proved that the high photo-catalytic activity was preserved after several reuse cycles, and there was evidence that no significant release of photocatalyst particles from PS pellets occurred.

Table 4. As(III) oxidation to As(V) over WO₃-based photocatalysts under visible light.

| Photocatalyst | pH | Light Source | As(III) (μM) | Catalyst (g/L) | As(III) Oxidized (%) | Time (min) | Ref. |
|---|----|--|--------------|----------------|----------------------|------------|------|
| Pt/WO ₃ | 3 | 300 W Xe arc lamp λ > 420 nm | 100 | 0.5 | 100 | 30 | [89] |
| WO ₃ | 3 | 300-W Xe arc lamp λ > 420 nm | 100 | 0.5 | 100 | 150 | [89] |
| (10 mg L ⁻¹ Cu ²⁺)/WO ₃ | 3 | visible LED light λ _{max} ~ 405 nm | 133 | 0.33 | 95 | 360 | [91] |
| (10 mg L ⁻¹ Cu ²⁺)/WO ₃ | 7 | visible LED light λ _{max} ~ 405 nm | 133 | 0.33 | 90 | 360 | [91] |
| 1 wt% CuO-WO ₃ | 10 | visible LED light λ _{max} ~ 405 nm | 133 | 0.33 | 80 | 360 | [91] |
| 1 wt% CuO-WO ₃ | 7 | visible LED light λ _{max} ~ 405 nm | 133 | 0.33 | 75 | 360 | [91] |

Table 5. As(III) oxidation to As(V) over ZnO-based photocatalysts under visible light.

| Photocatalyst | pH | Light Source | As(III) (μM) | Catalyst (g/L) | As(III) Oxidized (%) | Time (min) | Ref. |
|---|-----|--|--------------|----------------|----------------------|------------|------|
| 1.08 mol% Cu-doped ZnO | 7.2 | LED (10 W; light intensity 32 W/cm ²) 400–600 nm | 67 | 3 | 100 | 120 | [92] |
| 1.08 mol Cu-doped ZnO% supported on polystyrene pellets | 7.2 | LED (86 W; light intensity 78 mW/cm ²) 400–600 nm | 67 | n.a. | 100 | 120 | [93] |

Bismuth oxyhalides BiOX (X = Cl, Br, I) are promising photocatalysts under UV or visible-light illumination due to their layered structure, high activity, and stability. In several papers, BiOI, bismuth oxyiodide, as such or modified, was used as a photocatalyst for As(III) oxidation. In [94], the efficiency of BiOI was related to its morphology, which was in turn dependent on the viscosity of the solvent used in its synthesis. With the highest viscosity, largest specific surface area, and thinnest nanosheets with exposed (0 0 1) surfaces, it could efficiently absorb visible light, subsequently generate a large number of carriers, and then rapidly move to the nanosheet surface in the role of a static electric field, thereby yielding the highest photocatalytic efficiency. The proposed mechanism proceeds through the excitation of the BiOI nanoparticles under >420 nm illumination to excite electrons to the CB; these could reduce O₂ to O₂^{•-}, while the photogenerated holes cannot oxidize the hydroxyl groups due to unfavorable potential. Instead, they directly oxidize the As(III) adsorbed on the surface of BiOI.

Modifications included doping with La to obtain Bi_{0.9}La_{0.1}OI [95] to facilitate migration and hinder the recombination of photogenerated charge carriers. The contribution of La is due to free La³⁺ ions on the surfaces of BiOI nanosheets, which can form doping energy levels, trapping the photo-induced e⁻ below the CB edge of Bi_{0.9}La_{0.1}OI and accelerating the formation of O₂^{•-}. The in situ introduction of La into the lattice structure of BiOI

may provide more active sites for the formation of oxygen vacancies; these increase the amount of adsorbed oxygen and consequently induce the generation of superoxide radicals, suppressing the recombination of photogenerated electron–hole pairs, while the h^+ may migrate to the surface of $\text{Bi}_{0.9}\text{La}_{0.1}\text{OI}$.

ZrO_2 -modified $\text{BiOCl}_{0.5}\text{I}_{0.5}$ composites (ZBCI) [96] can not only oxidize As(III) into As(V) with visible-light irradiation but can also effectively capture the generated As(V), leading to negligible residual As(III) or As(V) in aqueous solutions after a 90 min treatment. In the fabricated composites, ZrO_2 acted as the main adsorption site, while $\text{BiOCl}_{0.5}\text{I}_{0.5}$ served as the primary photocatalysis center. Because of the hetero-structure of ZBCI, e^- generated by $\text{BiOCl}_{0.5}\text{I}_{0.5}$ would be transferred to ZrO_2 and an inhibited e^- - h^+ recombination rate, contributing to the improved photocatalytic efficiency. ZBCI can effectively remove As(III) over a broad pH range from 3 to 11. The high-resolution XPS spectra of ZBCI after the reaction showed that the As present on ZBCI surfaces was in the form of As(V), which further confirmed that As(III) was completely oxidized by photocatalysis.

$\text{BiOI@Fe}_2\text{O}_3$ core–shell nanoparticles [97] provided efficient removal of As(III) via a simultaneous photocatalytic oxidation–adsorption process with an As removal efficiency of 99.8% (3.99 mg/g) within 180 min. Such $\text{BiOI@Fe}_2\text{O}_3$ also demonstrated good As removal stability (3.8–4.0 mg/g) over a wide pH range of 2–8. Owing to the magnetic property, the $\text{BiOI@Fe}_2\text{O}_3$ nanocomposites can be rapidly recovered from the solution under an external magnetic field. $\text{Bi}_{2.15}\text{WO}_6$ (BWO) [98] can be used to treat wastewater containing both Mn(II) and As(III), as it can oxidize Mn(II) to amorphous manganese oxide (MnO_x) under visible light. MnO_x generated in this way can further transform As(III) to As(V). Conversion of As(III) to As(V) can be obtained either by the BWO-Mn(II) system under visible light or by the BWO- MnO_x system in the dark, with the latter system providing slightly better results. BWO can remove Mn(II) and As(III) via adsorption and/or oxidation processes. As(III) was gradually converted into As(V) as the reaction progressed, and the oxidation was basically complete after 24 h. The remaining As(III) was only 0.021 mg L^{-1} after the reaction, and the removal percentage was as high as 97.9%. The adsorbed As in the BWO- MnO_x system was mainly As(V). From the results reported in refs [97,98], although they are interesting, it is not possible to extrapolate the contribution of photooxidation versus absorption. To avoid inconsistencies with the other data in Table 6 (which refer to the oxidized amount), these results are omitted.

Table 6. As(III) oxidation to As(V) over bismuth oxide photocatalysts under visible light.

| Photocatalyst | pH | Light Source | As(III) (μM) | Catalyst (g/L) | As(III) Oxidized (%) | Time (min) | Ref. |
|---|------|---|---------------------------|----------------|----------------------|------------|------|
| $\text{Bi}_2\text{Sn}_2\text{O}_7$ | ~7.0 | 300 W halogen lamp 420–850 nm | 27 | 0.8 | 83 | 60 | [99] |
| BiOI | - | 300 W Xe lamp $\lambda > 420 \text{ nm}$ | 67 | 0.4 | 90 | 30 | [94] |
| ZrO_2 -coated $\text{BiOCl}_{0.5}\text{I}_{0.5}$ | 11 | Xe lamp $\lambda > 400 \text{ nm}$ | 67 | 0.25 | 90 | 60 | [96] |
| ZrO_2 -coated $\text{BiOCl}_{0.5}\text{I}_{0.5}$ | 7 | Xe lamp $\lambda > 400 \text{ nm}$ | 67 | 0.25 | 95 | 90 | [96] |
| $\text{Bi}_{1-x}\text{La}_x\text{OI}$ | 5.7 | 500 W Xe lamp $\lambda > 420 \text{ nm}$ | 133 | 1 | 90 | 150 | [95] |

Nanocrystalline $\text{Bi}_2\text{Sn}_2\text{O}_7$, with a band gap of 2.88 eV, exhibits a high photocatalytic activity in the oxidation of As(III) (up to 96.8%) under visible-light irradiation [99]. As(III) species can adsorb readily on the $\text{Bi}_2\text{Sn}_2\text{O}_7$ surface, which is beneficial for the subsequent oxidation of As(III) via photocatalyst. The total removal ratio of As(III) is up to 96.8% after 60 min of illumination.

3.4. Photocatalytic Oxidation of As(III) Using Graphitic Carbon Nitride Based Photocatalysts

Graphitic carbon nitride, often referred to as $g\text{-C}_3\text{N}_4$, recently gained significant attention owing to its distinct physicochemical characteristics. This layered structure, which is reminiscent of graphene, gained prominence for its stability, thermal resistance, and narrow band gap (around 2.7 eV). $g\text{-C}_3\text{N}_4$ comprises layers of bi-dimensional π -conjugated polymer structures, consisting of S-triazine or S-heptazine units and tertiary amine linkages. The appeal of $g\text{-C}_3\text{N}_4$ also stems from its environmental friendliness, straightforward preparation process, and cost-effectiveness. Nonetheless, pristine carbon nitride (pCN) exhibits limitations in terms of electronic conductivity, visible light absorption, and available surface active sites. These shortcomings were effectively addressed through diverse strategies, including the creation of heterojunctions, the introduction of heteroatoms, and nanostructural engineering. The material's photocatalytic efficacy under visible light sparked interest in applications involving hydrogen generation through water splitting and degradation of pollutants at room temperature.

Table 6 reports the entries of the results obtained using $g\text{-C}_3\text{N}_4$ in various forms to photocatalytically oxidize As(III) species.

Although $g\text{-C}_3\text{N}_4$ by itself can act as a photocatalyst, its performance in the oxidation of As(III) to As(V) species is poor in many conditions due to the rapid recombination of the photogenerated electron-hole pairs. A conversion as low as 5% was reported by Kim et al. [100], while other authors obtained conversions up to a maximum of about 65% [101] depending on the experimental conditions. Various modified types of $g\text{-C}_3\text{N}_4$ were usually able to improve the lifetime of the photogenerated species, reaching oxidation percentages of 41% [100], 67% [102], and 90% [101], and even complete oxidation in some cases [103,104].

For example, the oxidation ability was greatly enhanced in composite photocatalysts prepared by Wang et al. [103]: they produced a composite using bentonite clay by mixing and firing the two components at 450–550 °C, enhancing the oxidation capabilities of graphitic carbon nitride up to complete oxidation in 180 min of illumination with visible light, with only small changes in efficiencies by changing the solution pH from 3 to 8.5. The authors speculated that the improvement was caused by a change in the $g\text{-C}_3\text{N}_4$ structure in the composite, suggesting a negligible contribution of bentonite in the oxidation. Indeed, the oxidation ability was not linearly sensitive to the amount of bentonite (the 10% bentonite composite was the optimum composition, whereas the 5% and 20% composites had poorer performance). The structural change was also supported by the change in oxidation ability depending on the composite calcination temperature. Furthermore, a slight decrease in efficiency was observed when increasing the As(III) initial concentration.

The addition of amorphous iron to $g\text{-C}_3\text{N}_4$ was reported by Kim et al. [100] as a method of improving the removal ability of arsenic species in water. The photocatalysts were obtained in a single-step synthesis starting from melamine and iron and were compared with a mixture of $g\text{-C}_3\text{N}_4$ and crystalline hematite. The authors demonstrated a synergy between the oxidation of As(III) by the graphitic carbon nitride under illumination (both in UV and visible light) and the absorption of both As(III) and As(V) by the amorphous iron oxide species in the structure of the composite. Visible light seems to have a role in the process; nevertheless, the oxidation efficiency seems quite small (only about 40% of the absorbed As is in the form of As(V)), and the reported results seem mainly due to the absorption process; since the overall As removal is 41%, the oxidation efficiency can be calculated to be about 16%.

In 2017, Sun et al. [104] developed a $\alpha\text{-Fe}_2\text{O}_3/g\text{-C}_3\text{N}_4$ heterojunction, exploiting the relative positions of the conduction and valence bands of $\alpha\text{-Fe}_2\text{O}_3$ and $g\text{-C}_3\text{N}_4$ to allow the electrons in the CB of $g\text{-C}_3\text{N}_4$ to transfer to the CB of $\alpha\text{-Fe}_2\text{O}_3$, thus enhancing the lifetime of the photogenerated electron-hole pairs and inhibiting their rapid recombination. Indeed, the oxidation ability of the composite largely exceeded the ability of $g\text{-C}_3\text{N}_4$ alone (38%) and that of $\alpha\text{-Fe}_2\text{O}_3$ (21%). They found the optimum amount of $\alpha\text{-Fe}_2\text{O}_3$ in the composite

(8%) that allowed the oxidization of about 94% of the starting As(III) at neutral pH in 500 min of irradiation.

Wang et al. [101] used a different approach, modifying the g-C₃N₄ structure with pyromellitic diimide (PDI) doping. The modification gave rise to a high oxidation ability, so to produce high amounts of H₂O₂ in water. The photocatalyst was then applied to the simultaneous photooxidation of As(III) and photoreduction of Cr(VI) in high concentrations for the first time, so as to simulate Acid Mine Drainage composition. Nonetheless, we only analyze the results of As oxidation. At pH = 4 and after 120 min of visible light irradiation, the oxidation efficiency of As(III) reached 65% for the pure g-C₃N₄, which increased to a value of about 90% under the same conditions for the g-C₃N₄/PDI composite.

Later, Lei et al. [102] applied a different approach for a similar purpose: this time a direct Z-scheme photocatalyst was prepared by combining a magnetic semiconductor oxide ZnFe₂O₄ with g-C₃N₄ and, it was tested using simultaneous As(III) oxidation and Cr(VI) reduction. The as-prepared catalyst yielded a 67% oxidation of As(III) in two hours of reaction, starting from a mixture of both As(III) and Cr(VI). The result was enhanced by the addition of oxalate ions in the reaction mixture, obtaining virtually complete oxidation of As(III) in the same amount of time at pH = 5.

The same authors also employed a different approach using similar materials (core-shell structures of ZnFe₂O₄ supported on polyaniline (PANI) [105] that, for the sake of clarity, are analyzed in the following paragraph and reported in Table 7, together with other core-shell photocatalysts.

Table 7. As(III) oxidation to As(V) over g-C₃N₄-based photocatalysts.

| Photocatalyst | pH | Light Source | As(III) (μM) | Catalyst (g/L) | As(III) Oxidized (%) | Time (min) | Ref. |
|---|---------|-----------------------------|--------------|----------------|----------------------|------------|-------|
| Bentonite/g-C ₃ N ₄ | 3 ÷ 8.5 | 300 W Xe lamp | 133 | 0.2 | 100 | 180 | [103] |
| g-C ₃ N ₄ | 3 ÷ 8.5 | 300 W Xe lamp | 133 | 0.2 | 40 | 180 | [103] |
| Fe-g-C ₃ N ₄ | 7 | 400–680 nm | 334 | 5 | ~16 * | 300 | [100] |
| g-C ₃ N ₄ | 7 | 400–680 nm | 334 | 5 | <5 | 300 | [100] |
| α-Fe ₂ O ₃ /g-C ₃ N ₄ | 7 | 500 W Xe lamp | 67 | 0.5 | ~94 | 500 | [104] |
| g-C ₃ N ₄ /PDI ** | 4 | 300 W Xe lamp λ > 420 nm | 100 § | 1 | 90 | 120 | [101] |
| g-C ₃ N ₄ | 4 | 300 W Xe lamp λ > 420 nm | 100 § | 1 | 65 | 120 | [101] |
| ZnFe ₂ O ₄ /g-C ₃ N ₄ | 5 | n.a. | 60 § | 1 | 67 | 120 | [102] |
| ZnFe ₂ O ₄ /g-C ₃ N ₄ + oxalate | 5 | n.a. | 60 § | 1 | 100 | 120 | [102] |

* calculated as 37% of As(V) speciated on the catalyst that absorbed 41% of the starting As(III). ** pyromellitic diimide (PDI). § plus an equal amount of Cr(VI). n.a.= not available.

3.5. Photocatalytic Oxidation of As(III) Using Core–Shell Structure Photocatalysts

The approach of Lei et al. [105] involved the use of sulfate (SO₄^{•−}) and hydroxide (HO[•]) radicals, obtained by activation of sulfite radicals (SO₃^{•−}) via ZnFe₂O₄@PANI photocatalyst as the active species for As(III) oxidation. The efficacy of the photocatalyst was attributed by the authors to the core-shell structure of the catalyst. Indeed, the effect of PANI covering the ZnFe₂O₄ surface was emphasized by the increase in oxidation efficiency that spans from 60% with bare ZnFe₂O₄ to complete oxidation using ZnFe₂O₄@PANI in just 60 min. Moreover, the method is fairly independent of the solution pH in the range of 3–10, and the magnetic properties of the semiconductor oxide allow for easy recovery. A minor leaching of iron ions into the solution was reported, but less than observed for the bare ZnFe₂O₄.

Other core–shell structure catalysts that gained attention are silver-based compounds, especially silver halides, owing to their ability to absorb visible light and efficiently attain charge separation and charge transfer. In turn, core–shell structures allow for easy tunability of the catalyst properties.

Quin et al. [106] reported on the preparation and testing of Ag@AgCl core–shell nanowires. With an optimized composition, they obtained an oxidation efficiency of 40% in acidic conditions (pH = 3), 76% at neutral and 83% in basic conditions (pH = 10), after two hours of illumination (Table 8). The authors also tested the photocatalysts for several cycles, unfortunately showing a washout of the catalyst that decreased the efficiency to about 22% after 20 cycles.

Table 8. As(III) oxidation to As(V) over core–shell structured photocatalysts.

| Photocatalyst | pH | Light Source | As(III) (μM) | Catalyst (g/L) | As(III) Oxidized (%) | Time (min) | Ref. |
|--|--------|--|---------------------------|----------------|----------------------|------------|-------|
| ZnFe ₂ O ₄ | 3–10 | n.a. | 667 | 0.05 | 63 | 60 | [105] |
| ZnFe ₂ O ₄ @PANI* (+sulfite) | 3–10 | n.a. | 667 | 0.05 | ~100 | 60 | [105] |
| Ag@AgCl | 3/7/10 | 300 W halogen lamp $\lambda > 420$ nm | 27 | 0.3 | 40/76/83 | 120 | [106] |
| Ag@AgCl | 7 | 300 W Xenon lamp $420 < \lambda < 760$ nm | 27 | n.a. | ~39 | 180 | [107] |
| Fe-Ag@AgCl | 7 | 300 W Xenon lamp $420 < \lambda < 760$ nm | 27 | n.a. | ~92 | 180 | [107] |

* PANI: polyaniline. n.a.: not available.

The same authors also modified the pristine Ag@AgCl by incorporating iron [107] in a ratio of Ag:Fe = 1:1, which allowed for the reduction of the band gap of the photocatalyst from 3.25 eV to 3.04. They used the nanowire photocatalysts that were originally developed for the inactivation of *Escherichia coli* (*E. coli*) bacteria, in the concurrent oxidation of As(III) and inactivation of *E. coli*. The authors reported that the presence of the bacteria did not affect the efficiency of the catalyst on the photooxidation of As(III) until a very high amount (10^8 cfu/mL). The iron-modified photocatalyst resulted in an As(III) oxidation percentage of about 92% after 180 min of reaction under visible-light irradiation at neutral pH, increasing the performance of the iron-free photocatalyst, which, under the same conditions, only attained 39% oxidation.

4. Conclusions and Perspectives

In this review, the most advanced photocatalytic materials for arsenic removal are described with a focus on semiconductor catalysts activated by visible light, including the fundamental aspects of their design and applications. In addition, the importance of coupling materials for excellent oxidation of As(III) to As(V) by photocatalysis with highly adsorbent materials is highlighted. Figures 4 and 5 summarize the conclusions of the review in two radar charts. Figure 4 groups the best photocatalysts regardless of the working pH, while Figure 5 reports only the catalysts for which results were obtained at pH \approx 7. The radar charts allow the comparison of an arbitrary number of variables. The variables compared in these graphs are (clockwise, starting from the top): (i) [As(III)]: the molar concentration of As(III) used in the experiments in $\mu\text{mol/L}$ (μM). The lower the better, as the concentrations usually found in groundwater are very low and the limit for arsenic in drinking water is around 10 $\mu\text{g/L}$ (0.1 μM) [4]. (ii) [Catalyst]: the concentration of catalyst used (in mg/L). The lower the better (scale from 0 to 6 mg/L). (iii) Amount of As(III) oxidized to As(V) (in %): this is the efficiency of the photocatalyst in oxidizing As(III). The higher the better. (iv) Time (in minutes) required to attain the reported % of

As(III) oxidation. The lower the better. (v) pH: this is the specific pH condition at which the experiments were performed. The closer the pH is to 7 the better, the farther the pH deviates from 7 (either towards acidic or basic conditions), the worse.

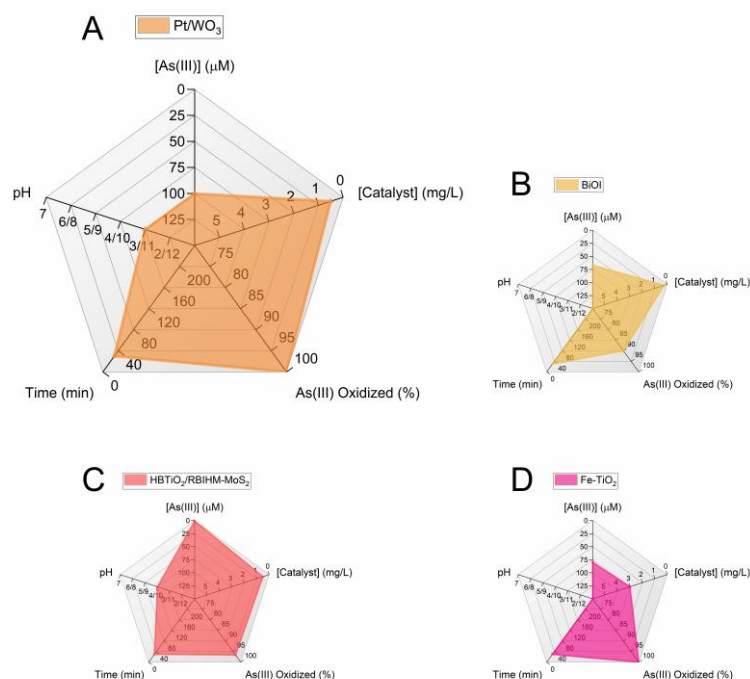


Figure 4. Radar graphs comparing the performance of the best visible-light photocatalytic systems. The first graph is enlarged to enhance the readability of the axis scales. The data used to prepare the figures refer to the following References: [89] (A); [94] (B); [81] (C); [68] (D).

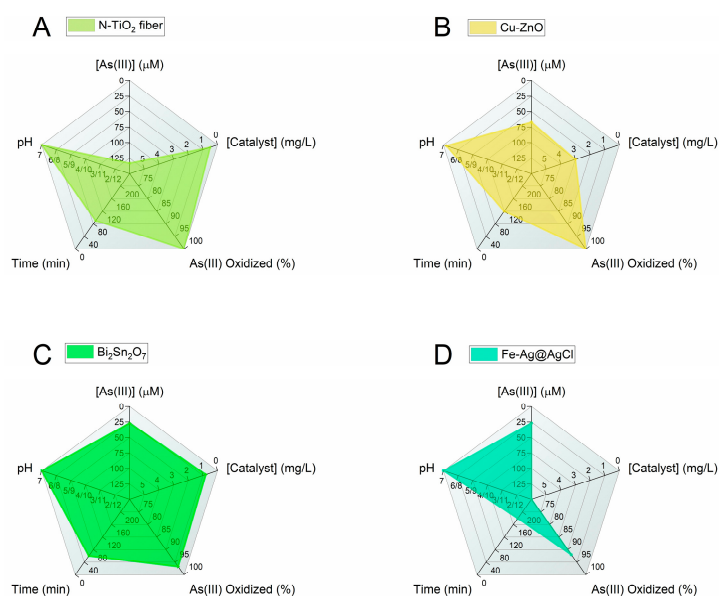


Figure 5. Radar charts comparing the performance of the best visible-light photocatalytic systems operating at pH \approx 7. References: [69] (A); [92] (B); [99] (C); [107] (D).

The scales of each variable are designed so that the better the catalyst, the larger the filled area in the graph. When data are unavailable, the parameter is assigned the worst possible value.

Currently, the most efficient performance under 30 min of visible-light irradiation is offered by the following photocatalysts (Figure 4): (1) Fe-doped TiO₂ with 100% As(III)

oxidation [68], HBTiO₂/RBIHM-MoS₂ with 96.6% As(III) oxidation [81], Pt/WO₃ with 100% As(III) oxidation [89], and BiOI with 90% As(III) oxidation [94]. It is worth noting that in these studies, the pH of the starting As(III) solution is 3 (Pt/WO₃) or 10 (HBTiO₂/RBIHM-MoS₂) or is not available (Fe-doped TiO₂, BiOI). For a practical application of the oxidation of As(III), it is necessary to work with an arsenic solution at a pH of approximately 7. Among the studies carried out at pH ≈ 7, the most interesting are the following (Figure 5): N-doped TiO₂ fiber with 100% As(III) oxidation under 90 min visible-light irradiation [69]; 1.08 mol% Cu-doped ZnO with 100% As(III) oxidation (120 min) [92]; Bi₂Sn₂O₇ with 83% As(III) oxidation (60 min) [99]; and Fe-Ag@AgCl with ~92% As(III) oxidation (180 min) [107]. These results show that long reaction time remains a major challenge in achieving high As oxidation.

For photocatalysis technology to find use in small low-resource communities, the photocatalyst must be robust and inexpensive. However, this cannot be the only criterion in the selection of a photocatalyst, as the effect of oxyanions, which are frequently present in water, on photocatalysis reaction rate through competitive adsorption and surface-site blocking can hinder As(III) oxidation.

Author Contributions: Conceptualization, I.N.S.; formal analysis, I.N.S., F.F., R.P. and B.B.; writing—original draft preparation, I.N.S., F.F., R.P. and B.B.; writing—review and editing, I.N.S., F.F. and R.P. All authors have read and agreed to the published version of the manuscript.

Funding: This research received no external funding.

Conflicts of Interest: The authors declare no conflicts of interest.

References

1. Sharma, V.K.; Sohn, M. Aquatic Arsenic: Toxicity, Speciation, Transformations, and Remediation. *Environ. Int.* **2009**, *35*, 743–759. [[CrossRef](#)] [[PubMed](#)]
2. Gupta, A.D.; Rene, E.R.; Giri, B.S.; Pandey, A.; Singh, H. Adsorptive and Photocatalytic Properties of Metal Oxides towards Arsenic Remediation from Water: A Review. *J. Environ. Chem. Eng.* **2021**, *9*, 106376. [[CrossRef](#)]
3. Sarkar, A.; Paul, B. The Global Menace of Arsenic and Its Conventional Remediation—A Critical Review. *Chemosphere* **2016**, *158*, 37–49. [[CrossRef](#)] [[PubMed](#)]
4. World Health Organization. *Exposure to Arsenic: A Major Public Health Concern; Preventing Disease through Healthy Environments*; World Health Organization: Geneva, Switzerland, 2019.
5. Singh, R.; Singh, S.; Parihar, P.; Singh, V.P.; Prasad, S.M. Arsenic Contamination, Consequences and Remediation Techniques: A Review. *Ecotoxicol. Environ. Saf.* **2015**, *112*, 247–270. [[CrossRef](#)] [[PubMed](#)]
6. Marinho, B.A.; Cristóvão, R.O.; Boaventura, R.A.R.; Vilar, V.J.P. As(III) and Cr(VI) Oxyanion Removal from Water by Advanced Oxidation/Reduction Processes—A Review. *Environ. Sci. Pollut. Res.* **2019**, *26*, 2203–2227. [[CrossRef](#)] [[PubMed](#)]
7. Shrestha, R.; Ban, S.; Devkota, S.; Sharma, S.; Joshi, R.; Tiwari, A.P.; Kim, H.Y.; Joshi, M.K. Technological Trends in Heavy Metals Removal from Industrial Wastewater: A Review. *J. Environ. Chem. Eng.* **2021**, *9*, 105688. [[CrossRef](#)]
8. Siddiqui, S.I.; Naushad, M.; Chaudhry, S.A. Promising Prospects of Nanomaterials for Arsenic Water Remediation: A Comprehensive Review. *Process Saf. Environ. Prot.* **2019**, *126*, 60–97. [[CrossRef](#)]
9. Kuroda, K.; Lu, B.; Hama, Y.; Yang, Y. Recent Progress in Photocatalysts for Oxidation of As(III) and Photocatalyst-Impregnated Adsorbents for Removing Aqueous Arsenic. *Curr. Opin. Environ. Sci. Health* **2023**, *35*, 100498. [[CrossRef](#)]
10. Issa, N.B.; Rajaković-Ognjanović, V.N.; Marinković, A.D.; Rajaković, L.V. Separation and Determination of Arsenic Species in Water by Selective Exchange and Hybrid Resins. *Anal. Chim. Acta* **2011**, *706*, 191–198. [[CrossRef](#)]
11. Wang, Z.; Fu, Y.; Wang, L. Abiotic Oxidation of Arsenite in Natural and Engineered Systems: Mechanisms and Related Controversies over the Last Two Decades (1999–2020). *J. Hazard. Mater.* **2021**, *414*, 125488. [[CrossRef](#)]
12. Nicomel, N.; Leus, K.; Folens, K.; Van Der Voort, P.; Du Laing, G. Technologies for Arsenic Removal from Water: Current Status and Future Perspectives. *Int. J. Environ. Res. Public Health* **2015**, *13*, 62. [[CrossRef](#)] [[PubMed](#)]
13. Liu, R.; Qu, J. Review on Heterogeneous Oxidation and Adsorption for Arsenic Removal from Drinking Water. *J. Environ. Sci.* **2021**, *110*, 178–188. [[CrossRef](#)] [[PubMed](#)]
14. Mahamallik, P.; Swain, R. A Mini-Review on Arsenic Remediation Techniques from Water and Future Trends. *Water Sci. Technol.* **2023**, *87*, 3108–3123. [[CrossRef](#)] [[PubMed](#)]
15. ALSamman, M.T.; Sotelo, S.; Sánchez, J.; Rivas, B.L. Arsenic Oxidation and Its Subsequent Removal from Water: An Overview. *Sep. Purif. Technol.* **2023**, *309*, 123055. [[CrossRef](#)]
16. Wang, Y.; Guo, C.; Zhang, L.; Lu, X.; Liu, Y.; Li, X.; Wang, Y.; Wang, S. Arsenic Oxidation and Removal from Water via Core-Shell MnO₂@La(OH)₃ Nanocomposite Adsorption. *Int. J. Environ. Res. Public Health* **2022**, *19*, 10649. [[CrossRef](#)] [[PubMed](#)]

17. Hug, S.J.; Leupin, O. Iron-Catalyzed Oxidation of Arsenic(III) by Oxygen and by Hydrogen Peroxide: pH-Dependent Formation of Oxidants in the Fenton Reaction. *Environ. Sci. Technol.* **2003**, *37*, 2734–2742. [[CrossRef](#)] [[PubMed](#)]
18. Sen Gupta, B.; Chatterjee, S.; Rott, U.; Kauffman, H.; Bandopadhyay, A.; DeGroot, W.; Nag, N.K.; Carbonell-Barrachina, A.A.; Mukherjee, S. A Simple Chemical Free Arsenic Removal Method for Community Water Supply—A Case Study from West Bengal, India. *Environ. Pollut.* **2009**, *157*, 3351–3353. [[CrossRef](#)] [[PubMed](#)]
19. He, X.; Lin, G.; Zeng, J.; Yang, Z.; Wang, L. Construction of Algal-Bacterial Consortia Using Green Microalgae *Chlorella vulgaris* and As(III)-Oxidizing Bacteria: As Tolerance and Metabolomic Profiling. *J. Environ. Sci.* **2024**, *139*, 258–266. [[CrossRef](#)] [[PubMed](#)]
20. Kraaijeveld, E.; Rijdsdijk, S.; Van Der Poel, S.; Van Der Hoek, J.P.; Rabaey, K.; Van Halem, D. Electrochemical Arsenite Oxidation for Drinking Water Treatment: Mechanisms, by-Product Formation and Energy Consumption. *Water Res.* **2024**, *253*, 121227. [[CrossRef](#)]
21. Syam Babu, D.; Nidheesh, P.V. A Review on Electrochemical Treatment of Arsenic from Aqueous Medium. *Chem. Eng. Commun.* **2021**, *208*, 389–410. [[CrossRef](#)]
22. Miao, X.; Shen, J.; Ji, W.; Zhang, T.C.; Liang, Y.; Yuan, S. Boosting Electrochemical Oxidation of As(III) on Fe-Doped RuO₂/PEDOT/SnO₂ Nanocomposite Anode: Fabrication, Performance and Mechanism. *J. Mater. Sci. Technol.* **2024**, *180*, 243–258. [[CrossRef](#)]
23. Litter, M.I.; Candal, R.J.; Meichtry, J.M. (Eds.) Reduction of Pentavalent and Trivalent Arsenic by TiO₂-Photocatalysis: An Innovative Way of Arsenic Removal. In *Advanced Oxidation Technologies*; CRC Press: Boca Raton, FL, USA, 2014; pp. 61–80, ISBN 978-0-429-22744-8.
24. Asere, T.G.; Stevens, C.V.; Du Laing, G. Use of (Modified) Natural Adsorbents for Arsenic Remediation: A Review. *Sci. Total Environ.* **2019**, *676*, 706–720. [[CrossRef](#)] [[PubMed](#)]
25. Hao, L.; Liu, M.; Wang, N.; Li, G. A Critical Review on Arsenic Removal from Water Using Iron-Based Adsorbents. *RSC Adv.* **2018**, *8*, 39545–39560. [[CrossRef](#)] [[PubMed](#)]
26. Mohan, D.; Pittman, C.U. Arsenic Removal from Water/Wastewater Using Adsorbents—A Critical Review. *J. Hazard. Mater.* **2007**, *142*, 1–53. [[CrossRef](#)] [[PubMed](#)]
27. Zhang, D.; Lin, J.; Luo, J.; Sun, S.; Zhang, X.; Ma, R.; Peng, J.; Ji, F.; Zheng, S.; Tian, Z.; et al. Rapid Immobilization of Arsenic in Contaminated Soils by Microwave Irradiation Combined with Magnetic Biochar: Microwave-Induced Electron Transfer for Oxidation and Immobilization of Arsenic (III). *Sci. Total Environ.* **2024**, *919*, 170916. [[CrossRef](#)]
28. Siddiq, O.M.; Tawabini, B.S.; Soupios, P.; Ntarlagiannis, D. Removal of Arsenic from Contaminated Groundwater Using Biochar: A Technical Review. *Int. J. Environ. Sci. Technol.* **2022**, *19*, 651–664. [[CrossRef](#)]
29. Sharma, P.K.; Kumar, R.; Singh, R.K.; Sharma, P.; Ghosh, A. Review on Arsenic Removal Using Biochar-Based Materials. *Groundw. Sustain. Dev.* **2022**, *17*, 100740. [[CrossRef](#)]
30. Foti, C.; Mineo, P.G.; Nicosia, A.; Scala, A.; Neri, G.; Piperno, A. Recent Advances of Graphene-Based Strategies for Arsenic Remediation. *Front. Chem.* **2020**, *8*, 608236. [[CrossRef](#)]
31. Shan, H.; Liu, Y.; Zeng, C.; Peng, S.; Zhan, H. On As(III) Adsorption Characteristics of Innovative Magnetite Graphene Oxide Chitosan Microsphere. *Materials* **2022**, *15*, 7156. [[CrossRef](#)]
32. Saqib, A.N.S.; Waseem, A.; Khan, A.F.; Mahmood, Q.; Khan, A.; Habib, A.; Khan, A.R. Arsenic Bioremediation by Low Cost Materials Derived from Blue Pine (*Pinus wallichiana*) and Walnut (*Juglans regia*). *Ecol. Eng.* **2013**, *51*, 88–94. [[CrossRef](#)]
33. Mondal, M.K.; Garg, R. A Comprehensive Review on Removal of Arsenic Using Activated Carbon Prepared from Easily Available Waste Materials. *Environ. Sci. Pollut. Res.* **2017**, *24*, 13295–13306. [[CrossRef](#)]
34. Olusegun, S.J.; Souza, T.G.F.; Mohallem, N.D.S.; Ciminelli, V.S.T. Removal and Environmentally Safe Disposal of As(III) and As(V)-Loaded Ferrihydrite/Biosilica Composites. *J. Environ. Manag.* **2023**, *335*, 117489. [[CrossRef](#)]
35. Hott, R.C.; Andrade, T.G.; Santos, M.S.; Lima, A.C.F.; Faria, M.C.S.; Bomfeti, C.A.; Barbosa, F.; Maia, L.F.O.; Oliveira, L.C.A.; Pereira, M.C.; et al. Adsorption of Arsenic from Water and Its Recovery as a Highly Active Photocatalyst. *Environ. Sci. Pollut. Res.* **2016**, *23*, 21969–21979. [[CrossRef](#)] [[PubMed](#)]
36. Taleb, K.; Markovski, J.; Milosavljević, M.; Marinović-Cincović, M.; Rusmirović, J.; Ristić, M.; Marinković, A. Efficient Arsenic Removal by Cross-Linked Macroporous Polymer Impregnated with Hydrous Iron Oxide: Material Performance. *Chem. Eng. J.* **2015**, *279*, 66–78. [[CrossRef](#)]
37. Carneiro, M.A.; Pintor, A.M.A.; Boaventura, R.A.R.; Botelho, C.M.S. Current Trends of Arsenic Adsorption in Continuous Mode: Literature Review and Future Perspectives. *Sustainability* **2021**, *13*, 1186. [[CrossRef](#)]
38. Ostermeyer, P.; Bonin, L.; Folens, K.; Verbruggen, F.; García-Timmermans, C.; Verbeken, K.; Rabaey, K.; Hennebel, T. Effect of Speciation and Composition on the Kinetics and Precipitation of Arsenic Sulfide from Industrial Metallurgical Wastewater. *J. Hazard. Mater.* **2021**, *409*, 124418. [[CrossRef](#)]
39. Moreira, V.R.; Lebron, Y.A.R.; Santos, L.V.S.; Coutinho de Paula, E.; Amaral, M.C.S. Arsenic Contamination, Effects and Remediation Techniques: A Special Look onto Membrane Separation Processes. *Process Saf. Environ. Prot.* **2021**, *148*, 604–623. [[CrossRef](#)]
40. Sodhi, K.K.; Kumar, M.; Agrawal, P.K.; Singh, D.K. Perspectives on Arsenic Toxicity, Carcinogenicity and Its Systemic Remediation Strategies. *Environ. Technol. Innov.* **2019**, *16*, 100462. [[CrossRef](#)]

41. Pranudta, A.; Patra, S.; Amonpattaratkit, P.; Klysubun, W.; Saiyasombat, C.; El-Moselhy, M.M.; Nguyen, T.T.; Padungthon, S. Immobilization of Arsenic in Wastewater from Regeneration of Fixed-Bed Adsorbent by Co-Precipitation with Zirconium Nano-Sludge for Disposal in Landfills. *J. Environ. Chem. Eng.* **2022**, *10*, 107756. [[CrossRef](#)]
42. Camacho, J.; Wee, H.-Y.; Kramer, T.A.; Autenrieth, R. Arsenic Stabilization on Water Treatment Residuals by Calcium Addition. *J. Hazard. Mater.* **2009**, *165*, 599–603. [[CrossRef](#)]
43. Zhang, H.; Yao, Q.; Shao, L.-M.; He, P.-J. Recovery of Arsenic Trioxide from a Sludge-Like Waste by Alkaline Leaching and Acid Precipitation. *Waste Biomass Valoriz.* **2014**, *5*, 255–263. [[CrossRef](#)]
44. Tian, J.; Wang, Y.; Zhang, X.; Sun, W.; Han, H.; Yu, Z.; Yue, T. A Novel Scheme for Safe Disposal and Resource Utilization of Arsenic-Alkali Slag. *Process Saf. Environ. Prot.* **2021**, *156*, 429–437. [[CrossRef](#)]
45. Siddique, T.; Gangadoo, S.; Quang Pham, D.; Dutta, N.K.; Choudhury, N.R. Antifouling and Antimicrobial Study of Nanostructured Mixed-Matrix Membranes for Arsenic Filtration. *Nanomaterials* **2023**, *13*, 738. [[CrossRef](#)] [[PubMed](#)]
46. Worou, C.N.; Chen, Z.-L.; Bacharou, T. Arsenic Removal from Water by Nanofiltration Membrane: Potentials and Limitations. *Water Pract. Technol.* **2021**, *16*, 291–319. [[CrossRef](#)]
47. Algeri, C.; Pugliese, V.; Coppola, G.; Curcio, S.; Calabro, V.; Chakraborty, S. Arsenic Removal from Groundwater by Membrane Technology: Advantages, Disadvantages, and Effect on Human Health. *Groundw. Sustain. Dev.* **2022**, *19*, 100815. [[CrossRef](#)]
48. Sharma, S.; Desai, A.V.; Joarder, B.; Ghosh, S.K. A Water-Stable Ionic MOF for the Selective Capture of Toxic Oxoanions of Se^{VI} and As^V and Crystallographic Insight into the Ion-Exchange Mechanism. *Angew. Chem. Int. Ed.* **2020**, *59*, 7788–7792. [[CrossRef](#)] [[PubMed](#)]
49. Padungthon, S.; German, M.; Wiriyathamcharoen, S.; SenGupta, A.K. Polymeric Anion Exchanger Supported Hydrated Zr(IV) Oxide Nanoparticles: A Reusable Hybrid Sorbent for Selective Trace Arsenic Removal. *React. Funct. Polym.* **2015**, *93*, 84–94. [[CrossRef](#)]
50. Bukhari, D.A.; Rehman, A. Metal-Resistant Bacteria as a Green Bioresource for Arsenic Remediation in Wastewaters. *Curr. Opin. Green Sustain. Chem.* **2023**, *40*, 100785. [[CrossRef](#)]
51. Kaya, C.; Uğurlar, F.; Ashraf, M.; Hou, D.; Kirkham, M.B.; Bolan, N. Microbial Consortia-Mediated Arsenic Bioremediation in Agricultural Soils: Current Status, Challenges, and Solutions. *Sci. Total Environ.* **2024**, *917*, 170297. [[CrossRef](#)]
52. Guo, J.; Luo, S.; Liu, Z.; Luo, T. Direct Arsenic Removal from Water Using Non-Membrane, Low-Temperature Directional Solvent Extraction. *J. Chem. Eng. Data* **2020**, *65*, 2938–2946. [[CrossRef](#)]
53. German, M.S.; Watkins, T.A.; Chowdhury, M.; Chatterjee, P.; Rahman, M.; Seingheng, H.; SenGupta, A.K. Evidence of Economically Sustainable Village-Scale Microenterprises for Arsenic Remediation in Developing Countries. *Environ. Sci. Technol.* **2019**, *53*, 1078–1086. [[CrossRef](#)] [[PubMed](#)]
54. Hossain, M.A.; Sengupta, M.K.; Ahamed, S.; Rahman, M.M.; Mondal, D.; Lodh, D.; Das, B.; Nayak, B.; Roy, B.K.; Mukherjee, A.; et al. Ineffectiveness and Poor Reliability of Arsenic Removal Plants in West Bengal, India. *Environ. Sci. Technol.* **2005**, *39*, 4300–4306. [[CrossRef](#)] [[PubMed](#)]
55. Sorensen, I.M.; McBean, E.A. Beyond Appropriate Technology: Social Considerations for the Sustainable Use of Arsenic-Iron Removal Plants in Rural Bangladesh. *Technol. Soc.* **2015**, *41*, 1–9. [[CrossRef](#)]
56. Hoffmann, M.R.; Martin, S.T.; Choi, W.; Bahnemann, D.W. Environmental Applications of Semiconductor Photocatalysis. *Chem. Rev.* **1995**, *95*, 69–96. [[CrossRef](#)]
57. Ryu, J.; Choi, W. Photocatalytic Oxidation of Arsenite on TiO₂: Understanding the Controversial Oxidation Mechanism Involving Superoxides and the Effect of Alternative Electron Acceptors. *Environ. Sci. Technol.* **2006**, *40*, 7034–7039. [[CrossRef](#)] [[PubMed](#)]
58. Fei, H.; Leng, W.; Li, X.; Cheng, X.; Xu, Y.; Zhang, J.; Cao, C. Photocatalytic Oxidation of Arsenite over TiO₂: Is Superoxide the Main Oxidant in Normal Air-Saturated Aqueous Solutions? *Environ. Sci. Technol.* **2011**, *45*, 4532–4539. [[CrossRef](#)] [[PubMed](#)]
59. Litter, M.I. Last Advances on TiO₂-Photocatalytic Removal of Chromium, Uranium and Arsenic. *Curr. Opin. Green Sustain. Chem.* **2017**, *6*, 150–158. [[CrossRef](#)]
60. García, F.E.; Litter, M.I.; Sora, I.N. Assessment of the Arsenic Removal From Water Using Lanthanum Ferrite. *ChemistryOpen* **2021**, *10*, 790–797. [[CrossRef](#)]
61. Molinari, R.; Argurio, P. Arsenic Removal from Water by Coupling Photocatalysis and Complexation-Ultrafiltration Processes: A Preliminary Study. *Water Res.* **2017**, *109*, 327–336. [[CrossRef](#)]
62. Pendlebury, S.R.; Wang, X.; Le Formal, F.; Cornuz, M.; Kafizas, A.; Tilley, S.D.; Grätzel, M.; Durrant, J.R. Ultrafast Charge Carrier Recombination and Trapping in Hematite Photoanodes under Applied Bias. *J. Am. Chem. Soc.* **2014**, *136*, 9854–9857. [[CrossRef](#)]
63. Tahir, M.; Tasleem, S.; Tahir, B. Recent Development in Band Engineering of Binary Semiconductor Materials for Solar Driven Photocatalytic Hydrogen Production. *Int. J. Hydrogen Energy* **2020**, *45*, 15985–16038. [[CrossRef](#)]
64. Pelaez, M.; Nolan, N.T.; Pillai, S.C.; Seery, M.K.; Falaras, P.; Kontos, A.G.; Dunlop, P.S.M.; Hamilton, J.W.J.; Byrne, J.A.; O’Shea, K.; et al. A Review on the Visible Light Active Titanium Dioxide Photocatalysts for Environmental Applications. *Appl. Catal. B Environ.* **2012**, *125*, 331–349. [[CrossRef](#)]
65. Jang, J.S.; Kim, H.G.; Lee, J.S. Heterojunction Semiconductors: A Strategy to Develop Efficient Photocatalytic Materials for Visible Light Water Splitting. *Catal. Today* **2012**, *185*, 270–277. [[CrossRef](#)]
66. Ochiai, T.; Fujishima, A. Photoelectrochemical Properties of TiO₂ Photocatalyst and Its Applications for Environmental Purification. *J. Photochem. Photobiol. C Photochem. Rev.* **2012**, *13*, 247–262. [[CrossRef](#)]
67. Lee, S.-Y.; Park, S.-J. TiO₂ Photocatalyst for Water Treatment Applications. *J. Ind. Eng. Chem.* **2013**, *19*, 1761–1769. [[CrossRef](#)]

68. Iervolino, G.; Vaiano, V.; Rizzo, L. Visible Light Active Fe-Doped TiO₂ for the Oxidation of Arsenite to Arsenate in Drinking Water. *Chem. Eng. Trans.* **2018**, *70*, 1573–1578. [[CrossRef](#)]
69. Zhang, G.; Sun, M.; Liu, Y.; Lang, X.; Liu, L.; Liu, H.; Qu, J.; Li, J. Visible-Light Induced Photocatalytic Activity of Electrospun-TiO₂ in Arsenic(III) Oxidation. *ACS Appl. Mater. Interfaces* **2015**, *7*, 511–518. [[CrossRef](#)] [[PubMed](#)]
70. Delgado-Diaz, D.; Hernandez-Ramirez, A.; Guzman-Mar, J.; Villanueva-Rodriguez, M.; Maya-Trevino, L.; Hinojosa-Reyes, L. N-S Co-Doped TiO₂ Synthesized by Microwave Precipitation Method: Effective Photocatalytic Performance for the Removal of Organoarsenic Compounds. *J. Environ. Chem. Eng.* **2021**, *9*, 106683. [[CrossRef](#)]
71. Ren, X.; Yao, H.; Tang, R.; Rong, A.; Yuan, S.; Wang, W.; Ali, I.; Hu, Z. Modification of TiO₂ by Er³⁺ and rGO Enhancing Visible Photocatalytic Degradation of Arsanilic Acid. *Environ. Sci. Pollut. Res.* **2022**, *30*, 35023–35033. [[CrossRef](#)]
72. Choi, W.; Yeo, J.; Ryu, J.; Tachikawa, T.; Majima, T. Photocatalytic Oxidation Mechanism of As(III) on TiO₂: Unique Role of As(III) as a Charge Recombinant Species. *Environ. Sci. Technol.* **2010**, *44*, 9099–9104. [[CrossRef](#)]
73. Ryu, J.; Choi, W. Effects of TiO₂ Surface Modifications on Photocatalytic Oxidation of Arsenite: The Role of Superoxides. *Environ. Sci. Technol.* **2004**, *38*, 2928–2933. [[CrossRef](#)] [[PubMed](#)]
74. Qin, Y.; Li, Y.; Tian, Z.; Wu, Y.; Cui, Y. Efficiently Visible-Light Driven Photoelectrocatalytic Oxidation of As(III) at Low Positive Biasing Using Pt/TiO₂ Nanotube Electrode. *Nanoscale Res. Lett.* **2016**, *11*, 32. [[CrossRef](#)] [[PubMed](#)]
75. Dutta, P.K.; Ray, A.K.; Sharma, V.K.; Millero, F.J. Adsorption of Arsenate and Arsenite on Titanium Dioxide Suspensions. *J. Colloid Interface Sci.* **2004**, *278*, 270–275. [[CrossRef](#)] [[PubMed](#)]
76. Ferguson, M.A.; Hoffmann, M.R.; Hering, J.G. TiO₂-Photocatalyzed As(III) Oxidation in Aqueous Suspensions: Reaction Kinetics and Effects of Adsorption. *Environ. Sci. Technol.* **2005**, *39*, 1880–1886. [[CrossRef](#)] [[PubMed](#)]
77. Zhao, D.; Xu, B.; Yang, J.; Wu, J.; Zhai, W.; Yang, B.; Liu, M. Rapid Preparation of TiO₂ and Its Photocatalytic Oxidation for Arsenic Adsorption under Visible Light. *Langmuir* **2020**, *36*, 3853–3861. [[CrossRef](#)] [[PubMed](#)]
78. González-Borrero, P.P.; Sato, F.; Medina, A.N.; Baesso, M.L.; Bento, A.C.; Baldissera, G.; Persson, C.; Niklasson, G.A.; Granqvist, C.G.; Ferreira Da Silva, A. Optical Band-Gap Determination of Nanostructured WO₃ Film. *Appl. Phys. Lett.* **2010**, *96*, 061909. [[CrossRef](#)]
79. Ezaki, M.; Kusakabe, K. Highly Crystallized Tungsten Trioxide Loaded Titania Composites Prepared by Using Ionic Liquids and Their Photocatalytic Behaviors. *Evergreen* **2014**, *1*, 18–24. [[CrossRef](#)]
80. Xie, L.; Liu, P.; Zheng, Z.; Weng, S.; Huang, J. Morphology Engineering of V₂O₅/TiO₂ Nanocomposites with Enhanced Visible Light-Driven Photofunctions for Arsenic Removal. *Appl. Catal. B Environ.* **2016**, *184*, 347–354. [[CrossRef](#)]
81. Balati, A.; Matta, A.; Nash, K.; Shipley, H.J. Heterojunction of Vertically Aligned MoS₂ Layers to Hydrogenated Black TiO₂ and Rutile Based Inorganic Hollow Microspheres for the Highly Enhanced Visible Light Arsenic Photooxidation. *Compos. Part B—Eng.* **2020**, *185*, 107785. [[CrossRef](#)]
82. Wang, Y.; Zhang, P.; Zhang, T.C.; Xiang, G.; Wang, X.; Pehkonen, S.; Yuan, S. A Magnetic γ -Fe₂O₃@PANI@TiO₂core-Shell Nanocomposite for Arsenic Removal via a Coupled Visible-Light-Induced Photocatalytic Oxidation-Adsorption Process. *Nanoscale Adv.* **2020**, *2*, 2018–2024. [[CrossRef](#)]
83. Ouyang, L.; Wang, Y.; Zhang, P.; Wang, X.; Yuan, S. Heterostructured MWCNTs@PANI@TiO₂ Nanocomposites for Enhanced Adsorption of As(III) from Aqueous Solution: Adsorption and Photocatalytic Oxidation Behaviors. *Ind. Eng. Chem. Res.* **2020**, *59*, 11743–11756. [[CrossRef](#)]
84. Wang, Y.; Zhang, Y.; Zhang, T.C.; Xiang, G.; Wang, X.; Yuan, S. Removal of Trace Arsenite through Simultaneous Photocatalytic Oxidation and Adsorption by Magnetic Fe₃O₄@PpPDA@TiO₂ Core-Shell Nanoparticles. *ACS Appl. Nano Mater.* **2020**, *3*, 8495–8504. [[CrossRef](#)]
85. Liu, X.; Wang, Y.; Zhang, T.; Xiang, G.; Wang, X.; Yuan, S. One-Pot Synthesis of a Magnetic TiO₂/PTh/Gamma-Fe₂O₃ Heterojunction Nanocomposite for Removing Trace Arsenite via Simultaneous Photocatalytic Oxidation and Adsorption. *Ind. Eng. Chem. Res.* **2021**, *60*, 528–540. [[CrossRef](#)]
86. Ouyang, L.; Zhang, Y.; Wang, Y.; Wang, X.; Yuan, S. Insights into the Adsorption and Photocatalytic Oxidation Behaviors of Boron-Doped TiO₂/g-C₃N₄ Nanocomposites toward As(III) in Aqueous Solution. *Ind. Eng. Chem. Res.* **2021**, *60*, 7003–7013. [[CrossRef](#)]
87. Bolognino, I.; Pelosato, R.; Marci, G.; Natali Sora, I. Comparison of Ten Metal-Doped LaFeO₃ Samples on Photocatalytic Degradation of Antibiotics in Water under Visible Light: Role of Surface Area and Aqueous Phosphate Ions. *Molecules* **2023**, *28*, 3807. [[CrossRef](#)]
88. Katz, A.; McDonagh, A.; Tijing, L.; Shon, H.K. Fouling and Inactivation of Titanium Dioxide-Based Photocatalytic Systems. *Crit. Rev. Environ. Sci. Technol.* **2015**, *45*, 1880–1915. [[CrossRef](#)]
89. Kim, J.; Lee, C.W.; Choi, W. Platinized WO₃ as an Environmental Photocatalyst That Generates OH Radicals under Visible Light. *Environ. Sci. Technol.* **2010**, *44*, 6849–6854. [[CrossRef](#)]
90. Kim, J.; Moon, G.; Kim, S.; Kim, J. Photocatalytic Oxidation Mechanism of Arsenite on Tungsten Trioxide under Visible Light. *J. Photochem. Photobiol. Chem.* **2015**, *311*, 35–40. [[CrossRef](#)]
91. Samad, A.; Furukawa, M.; Tateishi, I.; Katsumata, H.; Kaneco, S. Highly Efficient Visible Light-Induced Photocatalytic Oxidation of Arsenite with Nanosized WO₃ Particles in the Presence of Cu²⁺ and CuO. *Environ. Technol.* **2022**, *44*, 3096–3107. [[CrossRef](#)]
92. Vaiano, V.; Iervolino, G.; Rizzo, L. Cu-Doped ZnO as Efficient Photocatalyst for the Oxidation of Arsenite to Arsenate under Visible Light. *Appl. Catal. B Environ.* **2018**, *238*, 471–479. [[CrossRef](#)]

93. Vaiano, V.; Chianese, L.; Rizzo, L.; Iervolino, G. Visible Light Driven Oxidation of Arsenite to Arsenate in Aqueous Solution Using Cu-Doped ZnO Supported on Polystyrene Pellets. *Catal. Today* **2021**, *361*, 69–76. [[CrossRef](#)]
94. Hu, J.; Weng, S.; Zheng, Z.; Pei, Z.; Huang, M.; Liu, P. Solvents Mediated-Synthesis of BiOI Photocatalysts with Tunable Morphologies and Their Visible-Light Driven Photocatalytic Performances in Removing of Arsenic from Water. *J. Hazard. Mater.* **2014**, *264*, 293–302. [[CrossRef](#)] [[PubMed](#)]
95. Li, Z.; Wu, L.; Chen, M.; Zhang, Q.; Dai, S.; Zhao, T. Mechanochemical Construction of Bi_{1-x}LaxOI Solid Solution with Abundant Oxygen Vacancies for Enhanced Photocatalytic Oxidation of Inorganic/Organic Arsenic. *Appl. Surf. Sci.* **2022**, *602*, 154250. [[CrossRef](#)]
96. Ma, Z.; Zhang, M.; Guo, J.; Liu, W.; Tong, M. Facile Synthesis of ZrO₂ Coated BiOCl_{0.5}I_{0.5} for Photocatalytic Oxidation-Adsorption of As(III) under Visible Light Irradiation. *Chemosphere* **2018**, *211*, 934–942. [[CrossRef](#)] [[PubMed](#)]
97. Wang, Y.; Liu, X.; Chen, Q.; Zhang, T.C.; Ouyang, L.; Yuan, S. Simultaneous Photocatalytic Oxidation and Adsorption for Efficient As(III) Removal by Magnetic BiOI/ γ -Fe₂O₃ Core-Shell Nanoparticles. *Mater. Today Chem.* **2022**, *24*, 100823. [[CrossRef](#)]
98. Ren, H.-T.; Jing, M.-Z.; Liang, Y.; Li, T.-T.; Jiang, S.-M.; Lou, C.-W.; Lin, J.-H.; Han, X. Performance and Mechanism Involved in the Cascade Oxidation of Mn(II) and As(III) by Bi₂15WO₆ under Alkaline Conditions. *J. Environ. Chem. Eng.* **2021**, *9*, 106196. [[CrossRef](#)]
99. Tian, Q.; Zhuang, J.; Wang, J.; Xie, L.; Liu, P. Novel Photocatalyst, Bi₂Sn₂O₇, for Photooxidation of As(III) under Visible-Light Irradiation. *Appl. Catal. Gen.* **2012**, *425–426*, 74–78. [[CrossRef](#)]
100. Kim, J.-G.; Kim, H.-B.; Choi, J.-H.; Baek, K. Bifunctional Iron-Modified Graphitic Carbon Nitride (g-C₃N₄) for Simultaneous Oxidation and Adsorption of Arsenic. *Environ. Res.* **2020**, *188*, 109832. [[CrossRef](#)] [[PubMed](#)]
101. Wang, Z.; Murugananthan, M.; Zhang, Y. Graphitic Carbon Nitride Based Photocatalysis for Redox Conversion of Arsenic(III) and Chromium(VI) in Acid Aqueous Solution. *Appl. Catal. B Environ.* **2019**, *248*, 349–356. [[CrossRef](#)]
102. Lei, D.; Xue, J.; Peng, X.; Li, S.; Bi, Q.; Tang, C.; Zhang, L. Oxalate Enhanced Synergistic Removal of Chromium(VI) and Arsenic(III) over ZnFe₂O₄/g-C₃N₄: Z-Scheme Charge Transfer Pathway and Photo-Fenton like Reaction. *Appl. Catal. B Environ.* **2021**, *282*, 119578. [[CrossRef](#)]
103. Wang, C.; Dai, Y.; Fu, X.; Lu, H.; Zhang, J. A Novel Layer-Layer Crossed Structure of Bentonite/g-C₃N₄ for Enhanced Photocatalytic Oxidation of Arsenic(III) in a Wide pH Range. *Surf. Interfaces* **2021**, *26*, 101365. [[CrossRef](#)]
104. Sun, S.; Ji, C.; Wu, L.; Chi, S.; Qu, R.; Li, Y.; Lu, Y.; Sun, C.; Xue, Z. Facile One-Pot Construction of α -Fe₂O₃/g-C₃N₄ Heterojunction for Arsenic Removal by Synchronous Visible Light Catalysis Oxidation and Adsorption. *Mater. Chem. Phys.* **2017**, *194*, 1–8. [[CrossRef](#)]
105. Lei, D.; Xue, J.; Bi, Q.; Tang, C.; Zhang, L.; Zhang, J. Visible-Light Activation of Sulfite by ZnFe₂O₄@PANI Photocatalyst for As(III) Removal: The Role of Radicals and Fe(IV). *Appl. Surf. Sci.* **2022**, *578*, 151940. [[CrossRef](#)]
106. Qin, Y.; Cui, Y.; Tian, Z.; Wu, Y.; Li, Y. Synthesis of AG@AgCl Core-Shell Structure Nanowires and Its Photocatalytic Oxidation of Arsenic (III) Under Visible Light. *Nanoscale Res. Lett.* **2017**, *12*, 247. [[CrossRef](#)] [[PubMed](#)]
107. Cui, Y.; Ye, Q.; Wang, H.; Duo, X.; Peng, L.; Dong, W.; Cui, X.; Lu, Y.; Li, Y. Photocatalytic and Oxidation Mechanisms of Fe-Ag@AgCl: Effect on Co-Existing Arsenic (III) and *Escherichia coli*. *Environ. Res.* **2023**, *217*, 114913. [[CrossRef](#)]

Disclaimer/Publisher's Note: The statements, opinions and data contained in all publications are solely those of the individual author(s) and contributor(s) and not of MDPI and/or the editor(s). MDPI and/or the editor(s) disclaim responsibility for any injury to people or property resulting from any ideas, methods, instructions or products referred to in the content.